Computational Design and Validation Tests of Advanced-Concept Subsonic Inlets

T.J. Barber*
United Technologies Research Center, East Hartford, Connecticut
and
D.C. Ives,† D.P. Nelson,‡ and R. Miller§
Pratt & Whitney Aircraft Group, East Hartford, Connecticut

A NASA/industry cooperative program was established to develop new computational methodologies for subsonic inlet design and to demonstrate their application in the design of several configurations. The program produced three Pratt & Whitney designs that were tested at NASA Langley Research Center. The basic computational methods were corroborated by the test results through comparisons with the predicted surface pressure distributions as well as with the calculated total drag coefficient. Furthermore, the analysis and test program demonstrated that the use of laminar shock-free concepts in combination with an inverse analysis can produce performance improvements over conventionally designed inlets.

Nomenclature

A = area of control volume surface
A_∞ = area of capture streamtube
C_D = drag coefficient referenced to A_{MAX}
C_p = pressure coefficient
CR = convergence ratio of inlet
D = diameter of inlet at subscript location
L = length of inlet
m = mass flow rate per unit volume
M = Mach number
MFR = mass flow ratio, A_∞/A_{Hi}
p = static pressure
q = dynamic pressure
V = velocity
α = angle of attack

Subscripts

F = friction
FAN = fan face location
Hi = inlet highlight
MAX = maximum external diameter location
ST = stagnation condition
TOT = total traverse area
∞ = freestream conditions

Introduction

MODERN transport aircraft operating at cruise conditions typically encounter substantial regions of transonic flow on their wing and nacelle surfaces. The inlets on these nacelles have been conventionally designed using either the results from an experimentally obtained matrix of design conditions or from contours generated by analytic functions. Normally, experimental data are still used to define many of the undefined functional constants. The remaining coefficients are then manually adjusted in attempts to reduce the wave drag and skin-friction effects. When advanced-concept transport aircraft with their higher cruise Mach numbers and their higher-aspect-ratio supercritical wings are considered,[1,2] the problem of a proper inlet design becomes more critical. Efficiency considerations and the increased cost of testing are forcing designers to rely more heavily on computational methods. As a result, a cooperative NASA/industry program was established with Pratt & Whitney, Lockheed,[3] and General Electric[4] with the following objectives:

1) Develop computational procedures for the design of advanced-concept subsonic inlets.

2) Design a series of inlet contours corresponding to current and growth cycle gas turbine nacelle applications.

3) Obtain a detailed data base for code verification and for refining these new design concepts.

This paper will present three Pratt & Whitney (P&W) inlet designs. The text will describe the computational algorithms used in the design process and will present the experimental results of the NASA test program. Finally, the test data will be compared in detail to the analytic predictions obtained prior to the test phase of the program.

Computational Design Program

The design of engine inlets for subsonic transport aircraft must address a variety of performance parameters as well as geometrical constraints. Operational conditions ranging from low-speed, high-angle-of-attack flight at takeoff to high Mach number cruise in level flight must be considered. The inlet also has hard point constraints introduced—internally by the engine fan diameter and externally by the desired maximum wrap diameter D_{MAX}.

Evaluation of a given design is measured both in terms of its distributed surface loading as well as in terms of its integrated performance, the respective measures of which will be calculated surface pressure coefficient and the total drag. It is frequently more informative to break the total drag into components and thereby gain more insight toward improving the final design. The magnitude of these drag components varies in relative importance over the operating envelope of the inlet: the friction drag produced by boundary-layer growth dominates at low Mach numbers and, especially at high angles of attack, the wave drag due to shock losses dominates at high Mach numbers, and the pressure drag

Presented as Paper 84-1329 at the AIAA/SAE/ASME 20th Joint Propulsion Conference, Cincinnati, Ohio, June 11-13, 1984; received July 9, 1984; revision received Nov. 1, 1984.

*Senior Research Engineer. Member AIAA.
†Project Engineer. Member AIAA.
‡Analytical Engineer.
§Engineer. Member AIAA.

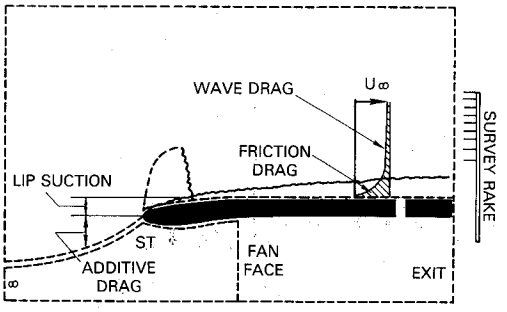

Fig. 1 Control volume definition for drag evaluation.

reflects the interaction of the boundary layer on the external pressure field.

The inviscid drag contribution is frequently[5] expressed in terms of alternate control volume components, one of which is the "additive" or "pre-entry drag" arising from the change in the momentum of the captured flow, while another is the lip suction force arising from overspeeding the flow over the forebody (inlet). When the cowl forebody suction force on the forward surface fails to compensate fully for the additive drag, the deficit is called a spillage drag. The total force is then obtained by taking a momentum balance over the control volume, which is defined by the upstream capture area, stagnation streamline, external surface, and exhaust or exit plane (see Fig. 1). In the following equation, the terms in the square brackets represent the thrust component and the remaining (negative) terms are the various components of the total drag:

$$C_{\text{FORCE}} = -C_{DF} - C_{DP} + \left[\frac{mv}{q} + C_p A\right]_{EX} - \left[\frac{mv}{q}\right]_{\infty}$$

$$- \int_{\infty}^{ST} C_p \, dA + \int_{ST}^{D_{\text{MAX}}} C_p \, dA - \int_{D_{\text{MAX}}}^{EX} C_p \, dA \qquad (1)$$

The first integral is called the additive drag and the second the lip suction component. The sum of these terms is the spillage drag. All three integrals represent the total inviscid or wave drag contribution obtained by integrating over the external contour. The additive drag can be evaluated by considering a momentum balance over the internal control volume bounded now by the inlet internal surface and the fan face, as

$$C_{DA} = C_{DINT} + \left[C_{p_{\text{FAN}}} \frac{A_{\text{FAN}}}{A_{Hi}} + 2\text{MFR}\left(\frac{V_{\text{FAN}}}{V_\infty} - 1\right)\right] \frac{A_{Hi}}{A_{\text{MAX}}} \qquad (2)$$

Experimental observations indicate that the external drag can be minimized by making both the maximum inlet diameter and the inlet forebody length L as small as possible, within the constraints imposed by the drag divergence and spillage mass flow ratio. It is interesting to note that the critical Mach number was found to correlate, among other parameters, to the thickness ratio of an equivalent ellipsoid.[6] This fact will be examined again below.

Typical design methodology incorporates these guidelines and constraints into a variety of polynomial representations for the inlet surface. Functional forms from parabolas to superellipses can be used, with the geometrical constraints of zero slope at D_{MAX} and infinite slope at the highlight eliminating two of the unknown coefficients. Several reliable inviscid computational methods[7-9] have then been used to optimize the remaining undetermined constants of the given functional form for a given set of performance criteria. Performance assessments can be made by including an interactive integral boundary-layer calculation through either a

Table 1 Inlet design parameters

Configuration	$\frac{D_{Hi}}{D_{\text{MAX}}}$	$\frac{L}{D_{\text{MAX}}}$	$\frac{D_{TH}}{D_{\text{MAX}}}$	CR	$\frac{A_{TH}}{A_{\text{FAN}}}$
P&W-1	0.867	0.502	0.775	1.25	0.863
P&W-2	0.886	0.300	0.793	1.25	0.799
P&W-3	0.867	0.502	0.775	1.25	0.863

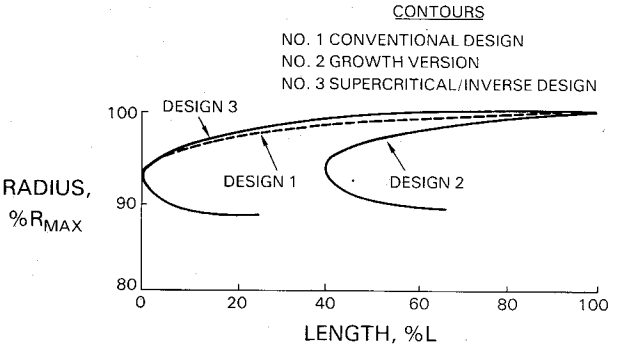

Fig. 2 Comparison of P&W subsonic inlet contours.

displacement surface or surface blowing procedure. The specific approach uses a Head's entrainment method[10] for the turbulent region, Gruschwitz's method[11] for the laminar region, and correlations by Dunham[12] and Hall and Gibbings[13] for the transition region. Recently, this approach was used to design a large L/D_{MAX} research-type inlet.[14] This design was included in this program (P&W-1) to provide a benchmark for the experimental portion of the program. A second more aggressive growth or short-duct inlet was also designed using the conventional approach (P&W-2). The design parameters for these inlets are summarized in Table 1. The primary problem with this design approach is that the computational techniques it incorporates are used only to optimize the drag characteristics of an inlet. On the other hand, design P&W-3 is based on an inverse design concept previously developed for supercritical isolated airfoils and compressor cascades.

The third inlet design attempted to use a recently introduced semidirect analysis to extend the performance range of a subsonic inlet by introducing supercritical and laminar flow considerations. Laminar control is obtained through pressure gradient control instead of external methods such as mechanically activated surface suction. For design 3, a shock-free design point C_p distribution is assumed that will maximize the lifting or suction force of the inlet, while avoiding the catastrophic effect of flow separation as the flow recompresses to the nacelle trailing edge. Local flow separation in the deceleration region is avoided if a Stratford-type C_p distribution is assumed. The specific algorithm[15] coupled any analysis algorithm (whether conservative or nonconservative full potential or Euler) to the driver in a semidirect fashion. The overall objectives of the aerodynamic design were to obtain high efficiency at the nominal design point of $M_\infty = 0.82$ and MFR = 0.70. Additional consideration had to be made to admit similar efficiencies over more extreme limits of the flight envelope, i.e., near the shock-free flow at $M_\infty = 0.82$ and MFR = 0.54 with no massive separation during low-speed climb operation. To achieve these objectives, a natural laminar flow/supercritical isentropic recompression was chosen as a goal. Since the largest contribution for a well-designed contour is friction related, a natural laminar flow was encouraged by accelerating the flow until the start of recompression. The recompression was specified to be isentropic to eliminate wave drag at the nominal design point. Specific geometric design constraints for the P&W-3 design were chosen so that the basic envelope

and internal contour would match the baseline of the P&W-1 design hard contraints. In particular, the internal contour from the highlight to the fan face and the external diameter at the metric break (D_{MAX}) were chosen to be identical with the P&W-1 design.

The contours of the three inlet designs are coplotted in Fig. 2. The atypical nature of the P&W-3 design is highlighted in a comparison of all the designs against the reference ellipsoid mentioned above. Figure 3 illustrates the different thickness distribution of P&W-3. By viewing contour variations in this manner, one can expand the highlight variations relative to a reference contour. The reference NACA-1 series inlet[16] is also included in the figure. The *predicted* performance of these inlets will be presented in the subsequent comparisons with experiment.

Experimental Program Description

The experimental phase of this program was conducted in the NASA Langley 16-ft transonic wind tunnel facility,[17,18] which is a single-return atmospheric facility with continuous air exchange. The test section is octangular in shape with axial slots at the wall vertexes. A throttle plug controlled the mass flow rate through the inlet, the actual rate being determined from pressure and temperature surveys at the inlet face location. The solid blockage of the model in the test section is between 0.88% (no flow through model) and 0.33% (throttle plug area only). Blockage effects of the exhaust flow are believed to become significant for Mach numbers greater than 0.85. The level of freestream turbulence has been measured to be less than 0.5% for the range of Mach number conditions of interest.[19]

All inlets were instrumented with 37 surface static pressure taps situated along the top and bottom dead center cuts. A connecting 1.5 D_{MAX} cylindrical section was used to mate the models with the support sting. Total pressure surveys using fixed rakes mounted 0.83 diameter aft of the model interface (metric break) were made to evaluate the drag characteristics of the various inlets. Drag balance data were originally intended as the primary source for drag data, but scatter in the data rendered this approach unreliable. However, the drag was determined from the following expression obtained by taking the appropriate external control volume as shown in Fig. 1. The drag data presented in the following section are primarily referenced to the metric break location; therefore, the rake data were analytically corrected to account for boundary-layer growth from the break to the traverse rake. A schematic of the test facility is shown in Fig. 4. The overall program investigated a large envelope of operating conditions for each inlet. In addition to the freestream Mach number and MFR variations, some limited angle-of-attack points were tested. Structural stability presented a large angle-of-attack study,

$$C_D = \sum_i \left[\frac{\dot{m}_i}{f(p_{0_i}/p_\infty)} \sqrt{\frac{T_{0_i}}{T_{0_\infty}}} \left(V - V_\infty\right) \frac{p_{0_i}}{q_\infty} \frac{A_i}{A_{MAX}} A_{TOT} - C_{p_i} \frac{A_i}{A_{MAX}} \right] \quad (3)$$

Boundary-layer characteristics of the inlet configurations were investigated using Acenaphthene flow visualization and leading-edge trip strips. In the first method, the transition is identified by a distinct change in the surface color from a clear to a darkened surface. The Reynolds number based on inlet length was approximately 4×10^6, that about one-tenth of that encountered by flight-type inlets. The flow visualization studies did confirm that substantial regions of laminar flow did exist on the untripped design 3 inlet, even at off-design conditions (low MFR). This is clearly seen in Fig. 5.

Comparisons and Analysis of Results

Comparisons between experimental data and analytic predictions are presented in this section. Although test data with and without trip strips are available for all inlets, only comparisons of clean inlets will be shown. Interpretation of the results and comments on the basic design approaches will be made after all of the data comparisons are presented. First, let us examine the detailed performance characteristics of the three inlets in terms of their surface pressure distributions. Comparisons with analysis are presented only for a limited set of flow conditions, specifically the design point and low MFR points were chosen to verify our computational design tools. The design point corresponds to a typical cruise operating condition for currently flying subsonic transport aircraft, while the low MFR condition corresponds to an axisymmetric simulation of engine-out operation (windmilling) during second segment climb. The pressure coefficient comparisons are presented in terms of an axial distance nondimensionalized with respect to the inlet length. Figures 6-8 include comparisons of test data with predicted results obtained from Euler, full potential nonconservative (FPNC), and full potential conservative (FPC) calculations for each

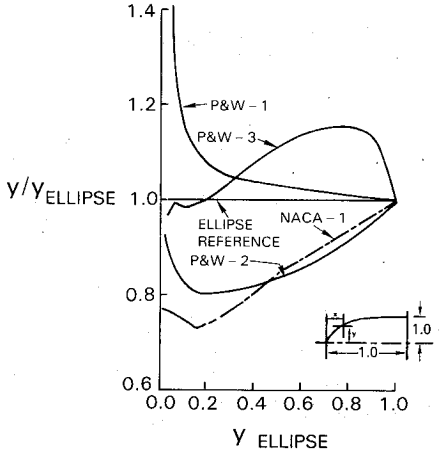

Fig. 3 Comparison of inlets relative to reference ellipse.

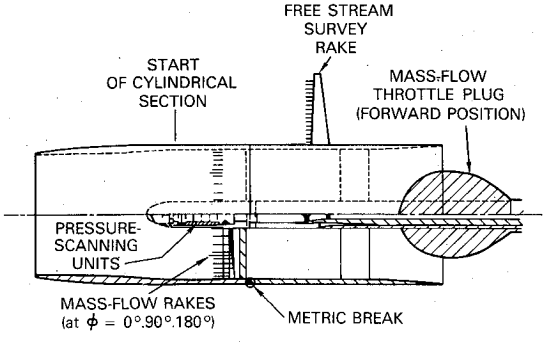

Fig. 4 Cross-sectional sketch of inlet model installation.

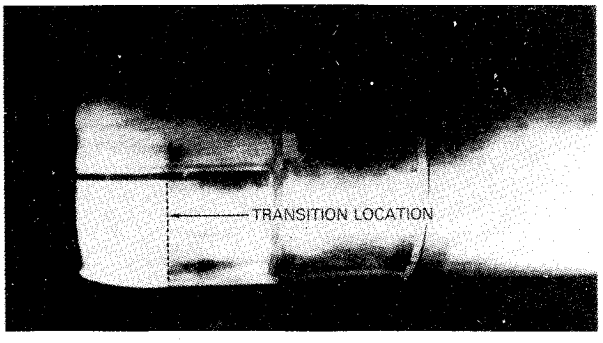

Fig. 5 Flow visualization of transition location on P&W-3 inlet.

inlet at their nominal design points. In these calculations, the interactive boundary-layer option was included; however, an examination of the pressure distribution showed little effect on them. The greatest shift occurred on the internal surface due to its adverse pressure gradient. The observed shifts are minor and can be attributed to the relatively high per foot Reynolds numbers of the cases. As a result, the effects of the viscous interaction will be ignored in the pressure comparisons, but will be included in the drag calculations. The agreement obtained with experiment is quite good for the methods shown. The predicted shock locations are axially ordered as expected, with the FPNC occurring first, then the Euler, and finally the FPC. In contrast to similar comparisons for isolated airfoils, the shock data more closely aligns to the Euler/FPC predictions. The FPC postshock spike should be expected from an ideal inviscid calculation.[20]

It is clear from Fig. 8 that the anticipated isentropic recompression was achieved in the third design while the "equivalent" inlet (P&W-1) has a strong shock. Further comparisons with experiment are given in Figs. 9 and 10 for the P&W-1 and -3 designs at a low mass flow ratio operating point. Substantially higher peak Mach numbers are observed in a narrow band near the highlight.

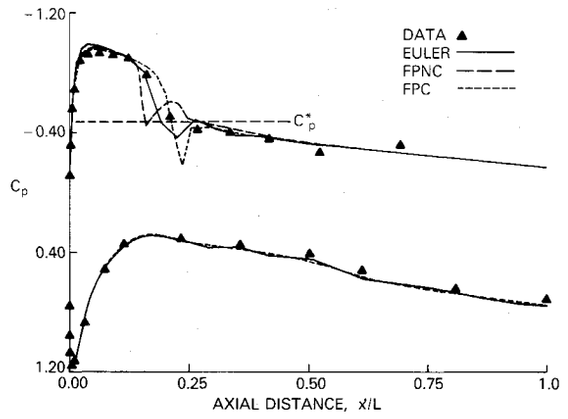

Fig. 6 Comparison of surface pressure coefficient prediction and measurement for P&W-1 inlet, $M_\infty = 0.793$, MFR = 0.691.

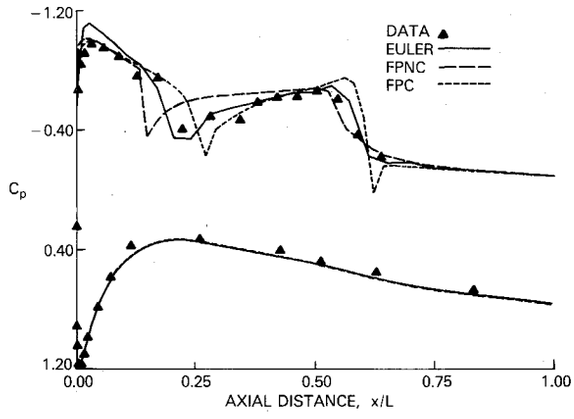

Fig. 7 Comparison of surface pressure coefficient prediction and measurement for P&W-2 inlet, $M_\infty = 0.695$, MFR = 0.576.

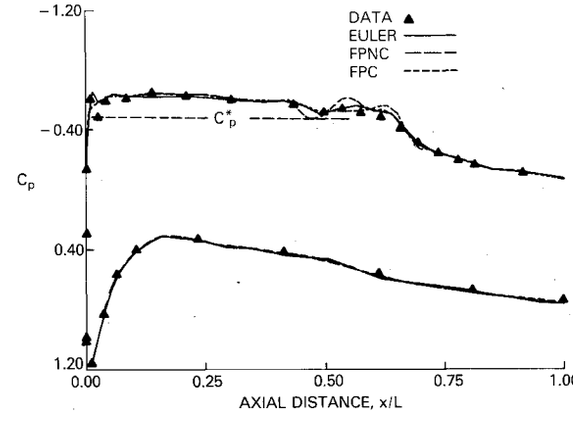

Fig. 8 Comparison of surface pressure coefficient prediction and measurement for P&W-3 inlet, $M_\infty = 0.792$, MFR = 0.688.

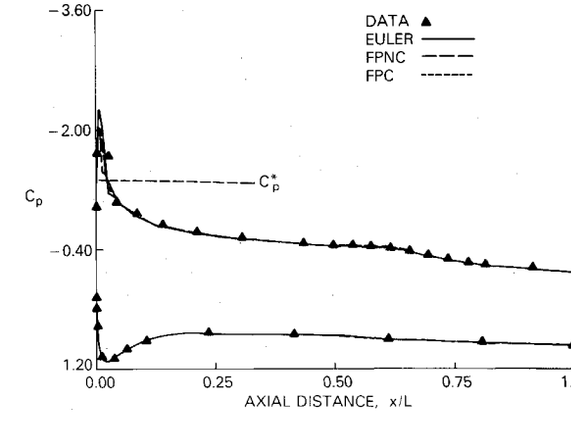

Fig. 9 Comparison of surface pressure coefficient prediction and measurement for P&W-1 inlet, $M_\infty = 0.596$, MFR = 0.493.

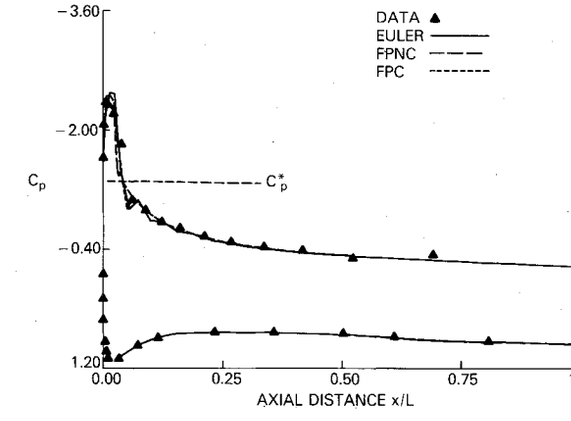

Fig. 10 Comparison of surface pressure coefficient prediction and measurement for P&W-3 inlet, $M_\infty = 0.593$, MFR = 0.491.

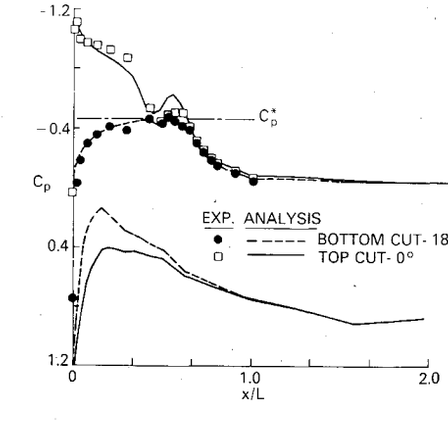

Fig. 11 Comparison of surface pressure coefficient prediction and measurement for P&W-3 inlet, $M_\infty = 0.79$, MFR = 0.69, $\alpha = 3.06$.

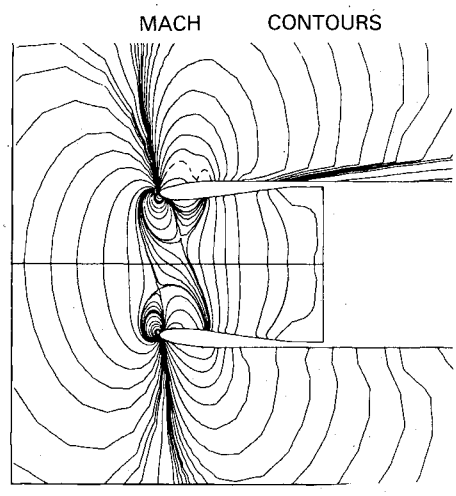

Fig. 12 Calculated Mach contours for P&W-3 inlet at angle of attack.

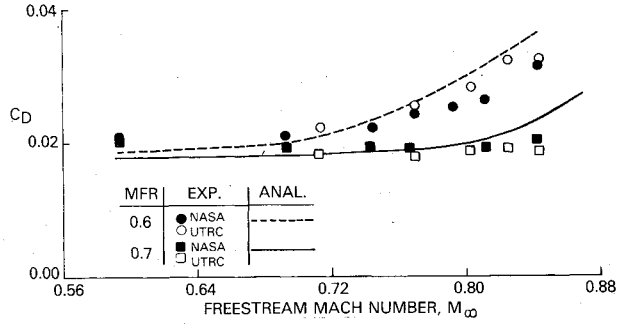

Fig. 13 Total drag comparisons for the P&W-1 inlet, MFR = 0.6, 0.7 (NASA and UTRC tests).

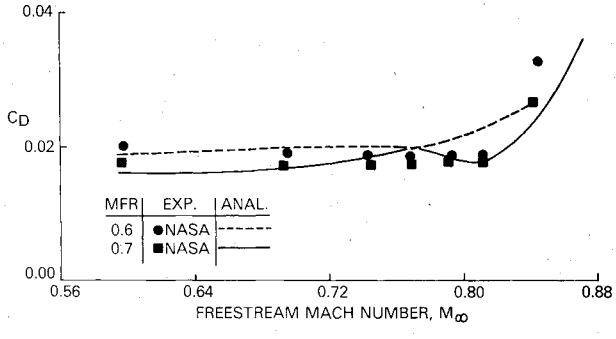

Fig. 14 Total drag comparisons for the P&W-3 inlet, MFR = 0.6, 0.7 (NASA and UTRC tests).

Before drawing conclusions from the results already presented, a single comparison between analysis and experiment is presented for inlet 3 at an angle of attack. The measured flow conditions of $\alpha = 3.06$, $M_\infty = 0.79$, and MFR = 0.69 were not corrected for any tunnel interference effects. The pressure calculations at the top and bottom dead center cuts, shown in Fig. 11, were made using a modified form of the Ni Euler method in three dimensions. The grid used was generated using a nearly conformal method.[22,23] Even though no viscous iteration is included, the agreement with experiment is still very good. A more complete visualization of the calculated flow asymmetry is seen through the Mach contours shown in Fig. 12. The dashed contour above the inlet identifies the sonic line. No such curve is shown on the lower surface since the flow is barely sonic.

Although all of the presented pressure distribution calculations accurately model the measured flowfield, no performance conclusions can be made without examining the drag

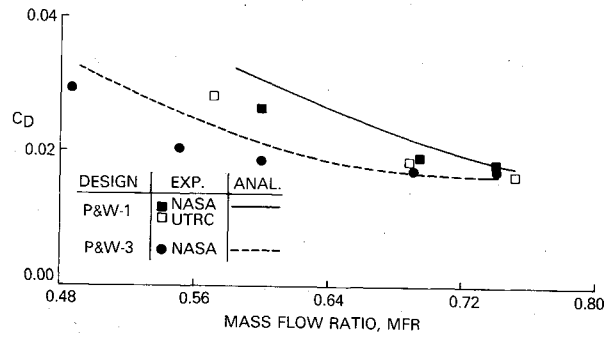

Fig. 15 Total drag comparisons vs MFR for P&W-1 and -3 inlets, $M_\infty = 0.811$ (NASA and UTRC tests).

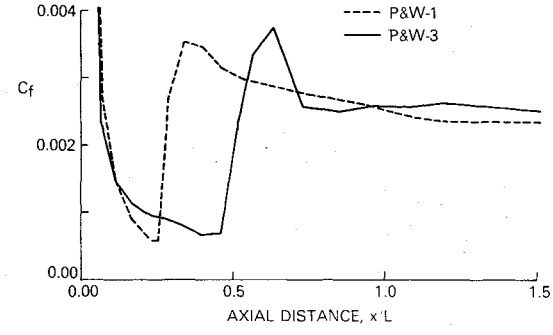

Fig. 16 Comparison of the calculated C_f distribution.

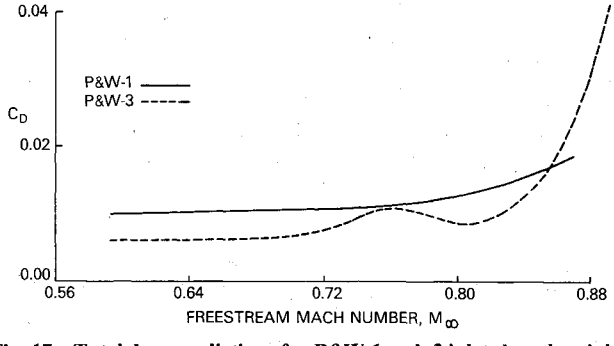

Fig. 17 Total drag predictions for P&W-1 and -3 inlets based on inlet length, MFR = 0.69.

characteristics of the inlets. The overall performance of the three inlets can best be interpreted through an examination of the integrated drag. Total drag calculations have been made using the FPNC method with the viscous iteration active. Drag comparisons with experiment are shown in Figs. 13 and 14 vs the freestream Mach number and in Fig. 15 vs the inlet mass flow ratio. The additional experimental data for the first inlet shown in these figures were obtained in an experiment performed at the United Technologies Research Center's transonic wind tunnel. In that earlier program, a sting-mounted model matching the design 1 contour was studied. The data from each facility were reduced from momentum rake measurements taken downstream of the metric break. The overall analysis/experiment agreement shown is again quite good. Although a stronger calculated total drag rise is indicated in Fig. 15, the relative difference between the performance of the two inlets is maintained.

A direct drag comparison of designs 1 and 3 at their design point is necessary to verify the efficacy of our new design approach. The results already cited somewhat mask such a comparison by the necessity of including the viscous drag

contribution produced by the interface to the traverse plane. Since friction effects dominate at cruise conditions, subtle differences in performance can be obscured by this effect. At the traverse plane, approximately two inlet lengths downstream of the metric break, the total friction drag contribution for designs 1 and 3 are approximately equal. Figure 16 illustrates that the laminar benefit of design 3 is negated by a slightly thicker boundary layer relative to design 1 over the cylindrical extension of the inlet. Recasting the previous results in terms of the inlet length alone produces the predictions in Fig. 17.

In this frame of reference, design 3 shows a 40 drag count (based on A_{MAX}) improvement over design 1. This translates approximately into a 0.67% thrust specific fuel consumption gain in engine efficiency. This benefit is lost as the operating point exceeds the design point, with the supercritical design producing a delayed but steeper drag rise than for design 1. The drag "bump" predicted in Figs. 14 and 17 initially was thought to be a wave drag effect arising from a weak double-shock pattern, commonly found in Korn-type airfoils,[21] but closer examination of the drag components showed no such wave drag contribution below $M_\infty = 0.81$. The bump can be traced to the interaction or pressure drag effects of the boundary layer on the external field. Since the experimental data exhibit no evidence of the drag "bump," it is believed to be an anomaly of the particular viscid coupling used in the FPNC calculation procedure.

A more difficult question to answer is the utility of using contouring rather than active surface suction to obtain laminar inlet flow. The analysis and NASA testing confirm that a significant performance benefit can be obtained from laminar designs, but the predicted boundary-layer difference at the metric break indicates that this benefit may be lost over the afterbody of a complete nacelle design. More radical contouring of the inlet can produce more extensive regions of laminar flow, but these designs typically result in thin highlight regions that have unacceptable performance characteristics at low-speed, high-angle-of-attack flight conditions. A more significant question to be answered is whether the improvements that were obtained and predicted for the model designs would still exist in flight-scale configurations. A more conclusive statement can be made only when a complete flight-scale nacelle is designed using the semidirect approach described here.

Conclusions

A cooperative subsonic inlet program was designed to verify computational methods so that they could be more effectively used in the design process. Furthermore, once these methods are calibrated, they were to be used as vehicles for investigating new design concepts. Examination of the presented surface pressure coefficient and total drag comparisons clearly shows that computational methods are available to predict inlet performance characteristics over a broad range of flight conditions. A more difficult question to be addressed is how these methods can be used to design for efficient inlet contours.

The P&W-3 inlet, designed using a semidirect analysis, considered two new design approaches simultaneously. This design combined a desired supercritical pressure distribution with an attempt at maintaining laminar flow over a significant portion of the inlet. The results shown in the previous section clearly demonstrate that these goals were achieved at the design point. The design 3 inlet drag had no wave drag contribution for freestream Mach numbers less than 0.82, but showed, as expected, a more rapid drag rise than produced by the conventional design 1.

References

[1] Presz, W.M. Jr., and Barber, T.J., "Computational Requirements for Efficient Engine Installation," AIAA Paper 84-0120, 1984.

[2] Henderson, W.P. and Patterson, J.C., "Propulsion Installation Characteristics for Turbofan Transports," AIAA Paper 83-0087, 1983.

[3] Vadyak, J. and Atta, E.H., "Three-Dimensional Transonic Nacelle/Inlet Flowfield Computations Using an Efficient Approximate Factorization Algorithm," AIAA Paper 83-1417, 1983.

[4] Younghans, J.L. and Lahti, D.J., "Experimental Studies on Natural Laminar Flow Nacelles," AIAA Paper 84-0034, 1984.

[5] Langley, M.J., "The Design of Axisymmetric Cowls for Podded Nacelles for High By-Pass Turbofan Engines," Aeronautical Research Council, Bedford, England, R&M No. 3846, 1979.

[6] Butler, S.F., "Aircraft Drag Prediction for Project Appraisal and Performance Estimation," AGARD CP-124, 1973.

[7] Caughey, D.A. and Jameson, A., "Accelerated Iterative Calculation of Transonic Nacelle Flows," *AIAA Journal,* Vol. 15, Oct. 1977, p. 1474.

[8] Ni, R.H., "A Multiple Grid Scheme for Solving the Euler Equations," *AIAA Journal,* Vol. 20, Nov. 1982, p. 1565.

[9] Jameson, A., Private communication, Princeton University, Princeton, N.J., Dec. 1979.

[10] Green, J.E., Weeks, D.J., and Brooman, J.W.F., "Prediction of Turbulent Boundary Layers and Wakes in Compressible Flow by a Lag-Entrainment Method," ARC R&M No. 3791, 1977.

[11] Schlichting, H., *Boundary Layer Theory,* 4th ed., McGraw-Hill Book Co., New York, 1960, pp. 356-363.

[12] Dunham, J., "Predictions of Boundary Layer Transition on Turbomachinery Blades," AGARD AG-164, 1972.

[13] Hall, D.J. and Gibbings, J.C., "Influence of Free-Stream Turbulence and Pressure Gradient Upon Boundary Layer Transition," *Journal of Mechanical Engineering, Science,* Vol. 14, 1972, pp. 134-146.

[14] Crook, J.L., Nelson, D.P., Wiley, R.H., and Presz, W.M., "Isolated Nacelle Performance-Measurement and Simulation," AIAA Paper 82-0134, 1982.

[15] Greeson, J.O., "Transonic Nacelle Tests in UTRC Large Subsonic Wind Tunnel," United Technologies Research Center, East Hartford, Conn., Rept. 80-56, 1980.

[16] Ives, D.C., "Supercritical Inlet Design," AIAA Paper 83-1866, 1983.

[17] Re, R.J., "An Investigation of Several NACA-1 Series Axisymmetric Inlets at Mach Numbers from 0.4 to 1.29," NASA RM X-2917, 1974.

[18] Corson, B.W., Runckel, J.F., and Igoe, W.B., "Calibration of the Langley 16-Foot Transonic Wind Tunnel with Test Section Air Removal," NASA TR R-423, 1971.

[19] Dougherty, N.S. Jr. and Steinle, F.W. Jr., "Transition Reynolds Number Comparison in Several Major Transonic Tunnels," AIAA Paper 74-0627, 1974.

[20] Gadd, G.E., "The Possibility of Normal Shock Waves on a Body with Convex Surfaces in Inviscid Transonic Flow," *ZAMP Brief Notes,* Vol. IX, 1960, p. 51.

[21] Bauer, F., Garabedian, P., and Korn, D., "Super-critical Wing Section III," *Lecture Notes in Economics & Mathematics Systems,* Vol. 150, Springer-Verlag, New York, 1977, p. 126.

[22] Ives, D.C., "Conformal Grid Generation," *Numerical Grid Generation,* edited by J.F. Thompson, Elsevier Publishing Co., New York, 1982.

[23] Ives, D.C., "Quasi-Three Dimensional Grid Generation Using Conformal Mapping," AIAA Paper 83-1906, 1983.